DE GRUYTER
OPEN

Growth and EPR properties of ErVO$_4$ single crystals

Grzegorz Leniec,
Sławomir M. Kaczmarek,
Marek Berkowski,
Michał Głowacki,
Tomasz Skibiński,
Bohdan Bojanowski

Abstract. Single crystals of ErVO$_4$ were grown by the Czochralski method under ambient pressure in a nitrogen atmosphere. Obtained crystals were transparent with strong pink coloring. Electron paramagnetic resonance (EPR) spectra were recorded as a function of the applied magnetic field. Temperature and angular dependences of the EPR spectra of the samples in the 3–300 K temperature range were analyzed applying both Lorentzian––Gauss approximation for diluted medium and Dyson for dense magnetic medium. EPR-NMR program was done to find local symmetry and spin Hamiltonian parameters of erbium ions.

Key words: dense magnetic medium • EPR • erbium • orthovanadate

G. Leniec✉, S. M. Kaczmarek, T. Skibiński,
B. Bojanowski
Institute of Physics,
Department of Mechanical Engineering
and Mechatronics,
West Pomeranian University of Technology,
48 Piastów Ave., 70-310 Szczecin, Poland,
E-mail: gleniec@zut.edu.pl

M. Berkowski, M. Głowacki
Institute of Physics of the Polish Academy of Sciences,
32/46 Lotników Ave., 02-668 Warsaw, Poland

Introduction

Rare-earth orthovanadates are birefringent crystals (e.g. refractive index of ErVO$_4$ is 0.227) and meet all necessary technical specifications to be a very prospective material for fiber optical communication systems [1–3]. They are also interesting due to their unusual magnetic characteristics and useful luminescent properties [4]. Er^{3+}:YVO$_4$ is one of the most promising laser hosts for micro- and diode-pumped solid-state lasers that exhibit a multisite character [4, 5]. ErVO$_4$ shows a high transmittance from visible to infrared region [6]. The crystals have the zircon structure and belong to the tetragonal space group $I4_1/amd$ (Fig. 1). Rare-earth ions occupy sites with local symmetry of D_{2d} [5–7].

Electron paramagnetic resonance (EPR) is a sensitive tool to study local environment around the probe ion and to estimate spin Hamiltonian parameters of rare-earth ions in host crystals. But it is worth remembering that the spin Hamiltonian parameters in diluted systems and concentrated ones usually differ from each other significantly [8]. Moreover, as was found by Misra $et\ al.$ [8], the EPR spectrum of the Er^{3+} ion in the mixed paramagnetic hosts Ho$_x$Y$_{1-x}$VO$_4$ could be clearly observed only for the samples with $x < 0.3$ and $x \geq 0.8$. For the samples with x in the region $0.3 < x < 0.8$, EPR spectra could not be observed due to complete broadening of EPR lines, presumably due to very short Er^{3+} relaxation times caused by the formation of percolation clusters.
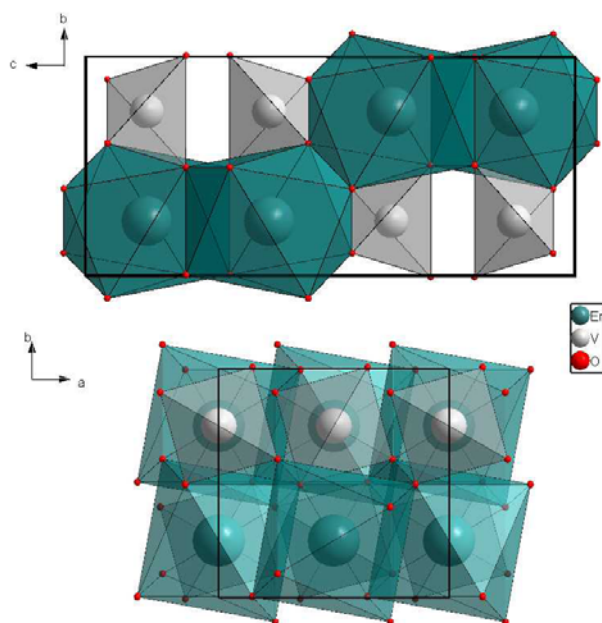
Fig. 1. The ErVO$_4$ single crystal structure seen in two different directions (according to crystallographic data from [7]).

Many papers were devoted to local sites symmetry description in YVO$_4$ slightly doped with erbium ions [1, 4–8], but a few only to EPR properties of concentrated ErVO$_4$ single crystals [8, 9]. In this paper, we focus our attention on the concentrated media to describe their magnetic properties using EPR spectroscopy.

The study of magnetic erbium ions is difficult due to the complex distribution of their energy levels. Erbium is a Kramers ion, $^4f_{11}$ electron configuration, and the ground state $^4I_{15/2}$.

The ground state of erbium is 16-fold degenerated. The ground state split into two doublets Γ^6, and Γ^7 with the effective spin $S = \frac{1}{2}$ ($g = 6.0$ (Γ^6) and $g = 6.8$ (Γ^7)), as well as three quartets Γ^8 with an effective spin $S = 3/2$. In the Er^{3+} surrounding of low symmetry, these quartets split into doublets, which is the source of strong Zeeman interaction anisotropy (Fig. 2) [10]. Experimental studies
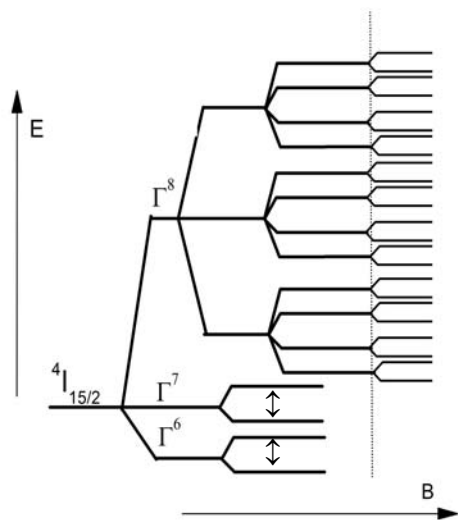

Fig. 2. The energy diagram of the ground state of Er^{3+} free ion.

show high magnetic anisotropy of *g* value, mainly (88%) due to dipole interaction. The very different *g* values indicate very complex interactions of the ground state and excited states. The EPR signal from Kramers Er^{3+} is observed only below ~50 K. The signal corresponds to the fine-structure Kramers-doublet transition (Γ^6 or Γ^7) for the ^{166}Er isotope with zero nuclear magnetic moment (abundance ~77%). The erbium ion has one stable odd isotope of mass 167, with 22.9% abundance and $I = 7/2$.

Experimental

Single crystals of ErVO$_4$ were grown by the Czochralski method in an inductively heated iridium crucible of 40 × 40 mm and with passive after heater. Starting materials with 4N purity were heated at 1000°C (Er$_2$O$_3$) or at 300°C (V$_2$O$_5$) for 6 hours before weighing, mixing, and melting. Due to evaporation of vanadium from the melt during crystal growth process [11], composition of starting oxides was 1 mol.% shifted toward a higher concentration of V$_2$O$_5$. Single crystals with 20-mm diameter were grown on a 2-mm iridium rod with a pulling rate of 3–4 mm/h and a rotation of 4–6 rpm. Crystals were grown under ambient pressure in a nitrogen atmosphere. During crystallization, a strong tendency to spiral growth was observed. In spite of the lack of crystal seed, most crystals started to grow along the direction close to *c* axis with *a* and *b* planes (cleavage planes) on the side. Obtained single crystals were transparent with strong pink coloring. In order to determine crystal quality, high-resolution X-ray diffraction measurements were performed using Siemens D5000 diffractometer (Ni-filtered CuKα radiation).

The samples used for EPR purposes have been shaped as 2.5 × 2.5 × 3.5 mm^3 parallelepipeds with planes perpendicular to crystallographic axes. The ESR spectra were recorded on a conventional X-band Bruker ELEXSYS E 500 CW-spectrometer operating at 9.5 GHz with a 100-kHz magnetic field modulation equipped with the standard helium gas flow system. The first crystal absorption spectra derivative was recorded as a function of the applied magnetic induction. In order to determine the local symmetry and localization of the paramagnetic probe in the crystal lattice, the angular dependences of Er^{3+} have been drawn.

Fitting of experimental data to spin Hamiltonian parameters was carried out using EPR-NMR program [12]. The program sets up a spin Hamiltonian matrix using the parameter matrices entered by the user, and then uses numerical diagonalization to produce the energy eigenvalues. The EPR-NMR was used to simulate the EPR spectra of erbium ion and for comparison with experimental data. All of the spin Hamiltonian parameters were obtained in such a way that the laboratory axis system corresponded to crystallographic axis system. Optimization and normalization (minimization) of the parameters was performed using root-mean-squared deviation method (RMSD).
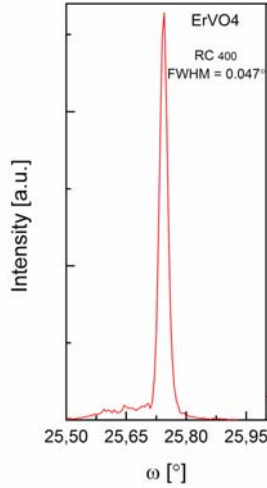
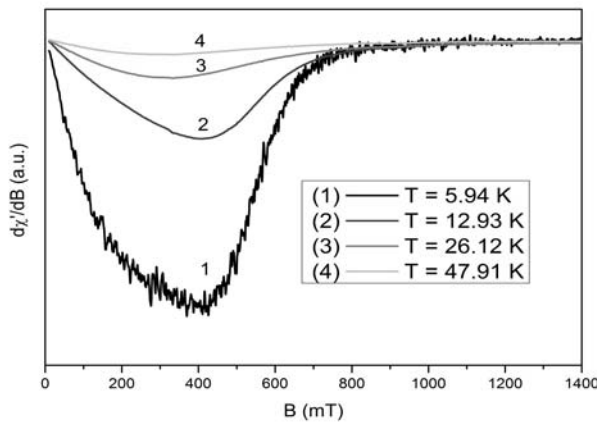**Fig. 3.** X-ray rocking curve for ErVO$_4$ single crystal.

Fig. 4. Temperature dependence of the EPR spectra of ErVO$_4$ single crystals.

Results and discussion

The X-ray rocking curve of ErVO$_4$ single crystal is presented in Fig. 3. It is obtained by analyzing the symmetrical (400) X-ray reflections. Full width at half maximum (FWHM) equals 0.047°. It indicates the good crystallographic quality of the investigated sample.

EPR spectra characteristic of the investigated crystals for several temperatures are presented in Fig. 4. As one can see, EPR signal is broad and asymmetric and suggests the presence of at least isolated or/and paired centers of Er^{3+} ions.

The EPR analysis was performed by applying two methods: classical one (LG – Lorentz–Gauss approximation) for diluted magnetic medium and special one, for magnetically dense medium whose EPR lines are broad and asymmetric. In a case of diluted medium for EPR line shape analysis, we applied the following equation [13]:

$$(1) \qquad \frac{d}{dB} P_{abs} = \frac{d}{dB} \left(\frac{1}{1 + \left(\left(B - B_{res}^{L} \right) \big/ \Delta B^{L} \right)^2} + \exp\left(- \left(\frac{B - B_{res}^{G}}{\Delta B^{G}} \right)^2 \ln 2 \right) \right)$$

where B is the applied magnetic field, B_{res} is the resonance line position, ΔB is the linewidth, indexes (L) and (G) describe Lorentz and Gauss shapes, respectively. Using Eq. (1) we were able to obtain parameters of spin Hamiltonian, dividing measured EPR line into three components assigned to erbium ions in different lattice positions.

In a case of dense magnetic medium, the EPR line shape analysis was performed using the following equation [14]:

$$(2) \qquad \frac{d}{dB} P_{abs} \approx \frac{d}{dB} \left(\frac{\Delta B + \alpha(B - B_{res})}{(B - B_{res})^2 + \Delta B^2} + \frac{\Delta B + \alpha(B + B_{res})}{(B + B_{res})^2 + \Delta B^2} \right)$$

where the main symbols in the equation are the same as in Eq. (1). New symbol, α, describes the asymmetry of EPR line. Such asymmetric line shapes are usually observed in metallic ferromagnetic materials, because of skin effect [14], as well as in the case of low symmetry magnets (the presence of nondiagonal elements of the dynamic susceptibility) [15, 16]. Due to the width and position of the EPR lines, positive and negative magnetic fields were taken into account.

Applying Eqs. (1) and (2), we have calculated angular dependences of EPR line resonance positions. The angular dependences for both types of media are very similar to each other. This allows us to use the same spin Hamiltonian for the dense and diluted magnetic medium. Calculation of the spin Hamiltonian parameters should allow the identification local symmetry of a paramagnetic center. The EPR lines positions could be analyzed using the following effective spin Hamiltonian [10, 17]:

$$(3) \qquad H = H_{\text{isolated}} + H_{\text{pair}}$$

where $H_{\text{isolated}} = \mu_B B \cdot g \cdot \tilde{S}$; H_{isolated} is an effective spin Hamiltonian for the isolated erbium ions with an effective spin $\tilde{S} = \frac{1}{2}$; μ_B is Bohr magneton, g is Zeeman splitting matrix; B is magnetic field; S is the spin operator.

$$(4) \qquad H_{\text{pair}} = \mu_B B \cdot g_i \cdot \tilde{S}_i + \mu_B B \cdot g_j \cdot \tilde{S}_j + \tilde{S}_i \cdot \tilde{D}_{ij} \cdot \tilde{S}_j$$

is an effective spin Hamiltonian of ion pairs (e.g., coupled Er^{3+} ions), where $S_i = S_j = \frac{1}{2}$ are effective spins for i, j ions and $g_i = g_j$ (assuming that the ions are similar and the principal axes of their g tensors are parallel), $\tilde{D}_{ij}$ is a general interaction matrix including all contributions to spin-spin interactions, whatever is their source. Such model allows for the good description of EPR spectra of ErVO$_4$ single crystal, taking into account also pairs with total spin $S = 1$.

Figure 5 shows the angular dependences of the resonance lines positions for ErVO$_4$ crystal in all crystallographic planes, *bc, ac, ab*, and at helium temperatures, in a whole range of crystal rotation. Besides experimental points, there are plotted solid (diluted medium) and dotted lines (dense medium) resulting from fitting procedure applying the EPR-
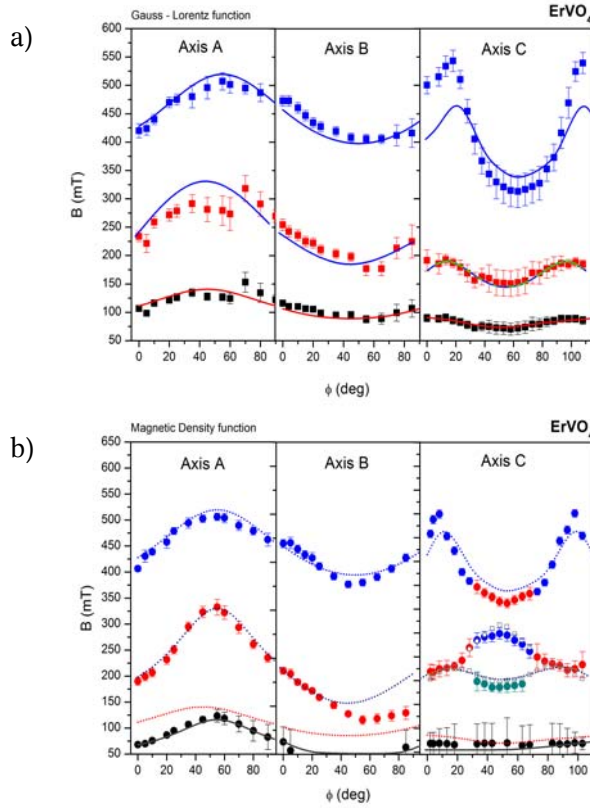
Fig. 6. Angular dependences of the EPR linewidth, ΔB.

Fig. 5. Angular dependences of resonance line positions measured when crystal is rotating perpendicularly to a, b, and c axis at temperatures $T = 8.2$, 6.9, and 7.85 K, respectively, in two cases: (a) diluted magnetic medium, (b) dense magnetic medium. Solid and dotted lines represent fitting parameters of the Hamiltonian according Eq. (3).

Fig. 7. Temperature dependence of EPR susceptibility, χ_{EPR}, calculated when crystal was rotated around c axis (ab plane). Solid line reflects Curie–Weiss law.

-NMR program [12]. From the figure, we were able to identify three different lines that are ascribed to erbium ions. First of the lines, observed in the lowest magnetic fields, we assigned to the isolated Er^{3+} ions, while two other lines, observed in higher magnetic fields we assigned to the pairs of Er^{3+} ions. As one can see, for both applied methods, points and lines assigned to the pairs of erbium ions correspond each other. The difference is only observed for points and lines assigned to isolated erbium ions, which can be understood as an effect of higher intensity of EPR signal originating from erbium pairs.

So, two kinds of paramagnetic centers are attributed to such a shape of angular dependences. Isolated erbium ions (lower lying line in Fig. 5) with an effective spin ½, and pairs of erbium ions (two higher lying lines in Fig. 5), each with an effective spin of ½ (total effective spin $S = 1$). The local symmetry of the isolated centers is D_{2d} (see Table 1) and the EPR signal originates from Γ^7 doublet, while the local symmetry of the pair centers is at least C_2. Because there is only small difference between an-

gular dependences derived using both methods, we decided to use one of them to calculate effective spin Hamiltonian parameters. By using Fig. 5a (diluted magnetic medium) and effective spin Hamiltonian described by Eqs. (3)–(5) and EPR-NMR program, we performed fittings of the angular dependences. The results of the fittings are presented in Fig. 5 as lines, and given in Table 1. The results indicate the high anisotropy of erbium paramagnetic centers and agree with other studies [18–21].

Angular dependences of the EPR linewidth for dense magnetic medium approximation, ΔB, are presented in Fig. 6. Similar angular dependence shows α parameter which was obtained by fitting experimental measurements to Eq. (2). It suggests that there is a strong correlation between asymmetry of the line and the width. The value of asymmetry parameter α is taken in a range of 0–1. Its value is due to a superposition of different types of interactions. It seems that the Eq. (2) can clearly reflect magnetic interactions only in a case of strong interactions (alpha different from zero). In a case of

Table 1. Parameters of g and $\widetilde{D}$ matrices for erbium centers calculated using effective spin Hamiltonian described by Eqs. (1)–(3) and EPR-NMR program [12]

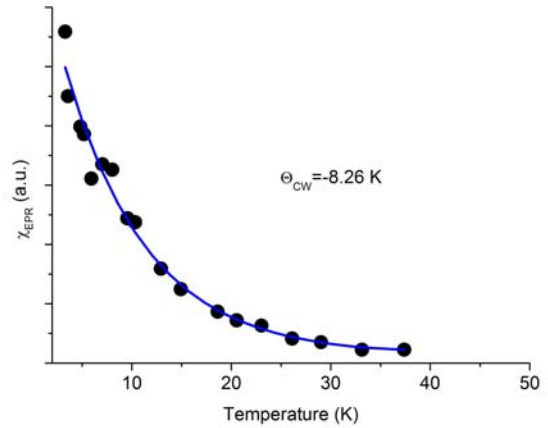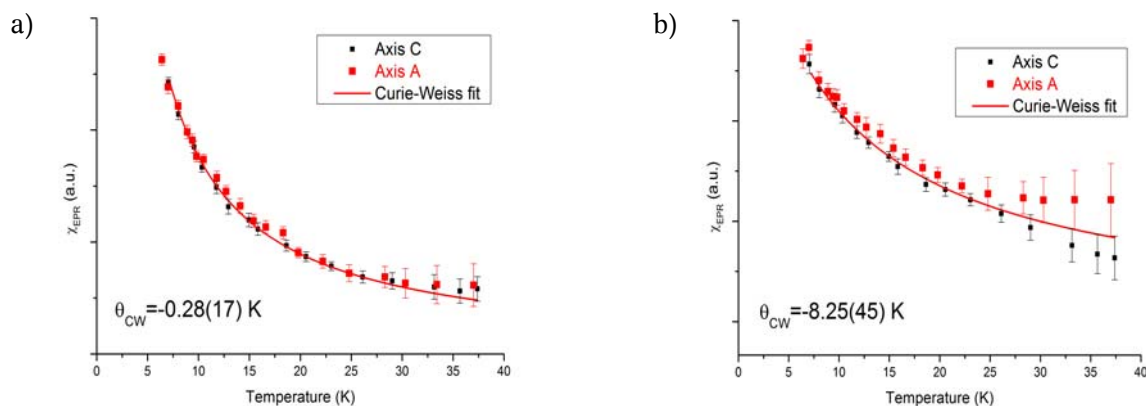|	$\bar{g} = 6.73(13)$		
$\mathbf{g}_{\text{isolated}}$ matrix	$g_x = 7.9(2)$	$g_y = 7.4(1)$	$g_z = 4.9(1)$
$\mathbf{g}_{\text{pairs}}$ matrix	$g_x = 2.41(10)$	$g_y = 1.54(5)$	$g_z = 1.13(5)$
$\widetilde{D}$ matrix [mT]	$D_x = 192(5)$	$D_y = 180(5)$	$D_z = 250(5)$

a)

b)

Fig. 8. Temperature dependence of EPR susceptibility calculated when crystal was along *c* and *a* axis, (a) isolated erbium center, (b) pair erbium centers. Solid line reflects Curie–Weiss law.

weak interactions, EPR signal is more symmetric, and more accurate results could be obtained from Lorentz–Gauss approximation (Eq. (1)).

Figure 7 shows temperature evolution of the integral intensity, χ_{EPR}, which is usually attributed to EPR magnetic susceptibility. It was calculated as a double integral of the EPR spectrum. As could be seen, ErVO$_4$ magnetic system fulfills Curie–Weiss (CW) relation: $\chi_{EPR} = C_0 + [C_1/(T - \theta_{CW})]$. Detailed calculation allowed to obtain the characteristic parameter $\theta_{CW} = -8.26$ K, where negative value indicates antiferromagnetic interactions between responsible magnetic centers. Solid line in Fig. 7 represents CW law, but in order to improve the fitting, we had to additionally take into account some diamagnetic component ($C_0 = 9.5 \times 10^{-5}$).

Figure 8 shows the temperature dependence of the EPR susceptibility, collected for the separated signals: isolated and pair erbium centers, drawn using data obtained applying Eq. (2). The results coincide with the ones obtained from the classical method. The interaction of both kinds of erbium centers is antiferromagnetic like. Isolated ions interacts weakly ($\theta_{CW} \sim -0.28$ K) while pairs much strongly ($\theta_{CW} \sim -8.25$ K). This confirms earlier conclusions resulting from analysis of angular dependences (Fig. 5, Table 1).

Isolated erbium ions (weakly interacting, $\theta_{CW} \sim -0.28$ K) substitute for yttrium ions just like low-doped orthovanadate crystals. Due to very similar ionic radii of erbium ($R = 103$ Å) and yttrium ($R = 104$ Å, [22]), they could occupy the same site symmetry. Erbium pairs ($\theta_{CW} \sim -8.25$ K) may be formed as a result of substitution of erbium ions at interstitial sites or as a result of their dislocation to one of crystallographic planes (chains). The latter supposition could also explain the appearance of additional EPR line registered along the *c* axis (see Fig. 5b).

Conclusions

Good quality ErVO$_4$ single crystals were grown by the Czochralski method. EPR spectroscopy was used for finding magnetic properties of the crystal. EPR lines are broad and asymmetric and vanish at about 50 K. Analysis of the spectra was possible for both kinds of approximation: dense and diluted magnetic medium, showing many similarities. It allowed for calculating spin Hamiltonian parameters for isolated and paired erbium ions, finding also local symmetry of the paramagnetic entities. It is D_{2d} for isolated erbium ions and lower, at least C_2, for pairs. Temperature dependences of the EPR spectra revealed the antiferromagnetic character of magnetic interactions in the crystal. Isolated erbium ions occupy positions of yttrium ions, while pairs of erbium ions are formed by the substitution of interstitial positions or the creation of dislocation planes.

References

1. Polosan, S., Bettinelli, M., & Tsuboi, T. (2007). Photoluminescence of Ho^{3+}:YVO$_4$ crystals. *Phys. Status Solidi (c)*, *4*(3), 1352–1355. DOI: 10.1002/pssc.200673749.
2. Ohlsson, N., Krishna, R. M., & Kroll, S. (2002). Quantum computer hardware based on rare-earth--ion-doped inorganic crystals. *Opt. Commun.*, *201*, 71–77. DOI: 10.1016/S0030-4018(01)01666-2.
3. Terada, Y., Shimamura, K., Kochurikhin, V. V., Barashov, L. V., Ivanov, M. A., & Fukuda, T. (1996). Growth and optical properties of ErVO$_4$ and LuVO$_4$ single crystals. *J. Cryst. Growth*, *167*, 369–372. DOI: 10.1016/0022-0248(96)00407-1.
4. Guillot-Noel, O., Simons, D., & Gourier, D. (1999). EPR study of the multisite character of Nd^{3+} ions in zircon-type matrices YMO$_4$ (M = V, P, As). *J. Phys. Chem. Solids*, *60*, 555–565. DOI: 10.1016/S0022-3697(98)00299-6.
5. Misra, S. K., Isbe, S., Capobianco, J. A., & Cavalli, E. (1999). Electron paramagnetic resonance of Er^{3+} doped in YVO$_4$: hyperfine parameters. *Chem. Phys.*, *240*, 313–318. DOI: 10.1016/S0301-0104(98)00393-0.
6. Will, G., Lugscheider, W., Zinn, W., & Patscheke, E. (2006). Neutron diffraction and susceptibility measurements on ErPO$_4$ and ErVO$_4$. *Solid State Phys.*, *46*(2), 597–601. DOI: 10.1002/pssb.2220460216.
7. Range, K., & Meister, H. (1990). ErVO$_4$-II, a scheelite--type high-pressure modification of erbium orthovanadate. *Acta Crystallogr. C-Cryst. Struct. Commun.*, *46*, 1093–1094. DOI: 10.1107/S0108270189014162.
8. Misra, S. K., & Andronenko, S. I. (2001). EPR study of Er^{3+} crystal-field and Ho-165(3+)-Er^{3+} interactions in single crystals of Ho$_x$Y$_{1-x}$VO$_4$ (x=0.02-1.00).

Phys. Rev. B, *64*, 094435-8. DOI: 10.1103/Phys-RevB.64.094435.

9. Misra, S. K., & Andronenko, S. I. (1996). Effect of host paramagnetic ions on the Gd^{3+} EPR linewidth in diluted Van-Vleck paramagnets $Tm_xLu_{1-x}PO_4$ and $Ho_xY_{1-x}VO_4$ and EPR spectra of Er^{3+} in $Ho_xY_{1-x}VO_4$ *Phys. Rev. B*, *53*, 11631–11641. DOI: 10.1103/ PhysRevB.53.11631.

10. Abragam, A., & Bleanely, B. (1970). *Electron paramagnetic resonance of transition ions*. London: Oxford University Press.

11. Oka, K., Unoki, H., Shibata, H., & Eisaki, H. (2006). Crystal growth of rare-earth orthovanadate (RVO_4) by the floating-zone method. *J. Cryst. Growth*, *286*, 288–293. DOI: 10.1016/j.jcrysgro.2005.08.058.

12. Mombourquette, M. J., Weil, J. A., & McGavi, D. G. (1999). *EPR-NMR User's manual*. Saskatoon, Canada: Department of Chemistry, University of Saskatchewan.

13. Pool, C. P., & Farach, H. A. (1979). Lineshapes in electron spin resonance. *Bull. Magn. Reson.*, *1*(4), 162–194.

14. Dyson, F. J. (1955). Electron spin resonance absorption in metals. II. Theory of electron diffusion and the skin effect. *Phys. Rev.*, *98*, 337–359. DOI: 10.1103/ PhysRev.98.349.

15. Benner, H., Brodehl, M., Seitz, H., & Wiese, J. (1983). Influence of nondiagonal dynamic susceptibility on the EPR signal of Heisenberg magnet. *J. Phys. C-Solid State Phys.*, *16*, 6011–6030. http://iopscience.iop.org/0022-3719/16/31/015.

16. Choukroun, J., Richard, J. -L., & Stepanov, A. (2003). Electron paramagnetic resonance in weakly anisotropic Heisenberg magnets with a symmetric anisotropy. *Phys. Rev. B*, *68*, 144415-10. DOI: 10.1103/Phys-RevB.68.144415.

17. Weil, J. A., & Bolton, J. R. (2007). *Electron paramagnetic resonance*. Hoboken, New Jersey: John Wiley & Sons Inc.

18. Ranon, U. (1968). Paramagnetic resonance of Nd^{3+}, Dy^{3+}, Er^{3+} and Yb^{3+} in YVO_4. *Phys. Lett. A*, *28*, 228–229. DOI: 10.1016/0375-9601(68)90218-1.

19. Bravo, D., Martin, A., & Lopez, F. J. (1999). A new EPR centre of Er^{3+} in MgO or ZnO co-doped $LiNbO_3$ single crystals. *Solid State Commun.*, *112*, 541–554. DOI: 10.1016/S0038-1098(99)00395-6.

20. Misra, S. K., Chang, Y., & Felsteiner, J. (1997). A calculation of effective g-tensor values for R^{3+} ions in $RBa_2Cu_3O_7$-δ and $RBa_2Cu_4O_8$ (R = rare earth): Low temperature ordering of rare-earth moments. *J. Phys. Chem. Solids*, *58*, 1–11. DOI: 10.1016/S0022-3697(96)00110-2.

21. Chai, R. -P., Kuang, X. -Y., Li, C. -G., & Zhao, Y. -R. (2011). Theoretical studies of EPR spectra and defect structure for three Er^{3+} centers in thorium dioxide. *Chem. Phys. Lett.*, *505*, 65–70. DOI: 10.1016/j.cplett.2011.02.013.

22. Shannon, R. D. (1976). Revised effective ionic radii and systematic studies of interatomic distances in halides and chalcogenides. *Acta Crystallogr. Sect. A*, *32*, 751–767. DOI: 10.1107/S0567739476001551.